Coupling of Photon Emitters in Monolayer WS$_2$ with a Photonic Waveguide Based on Bound States in the Continuum

Xiao-Jing Liu,[△] Yue Yu,[△] Di Liu, Qi-Long Cui, Xiaozhuo Qi, Yang Chen, Guangyuan Qu, Li Song, Guo-Ping Guo, Guang-Can Guo, Xiankai Sun,* and Xi-Feng Ren*

Cite This: *Nano Lett.* 2023, 23, 3209−3216
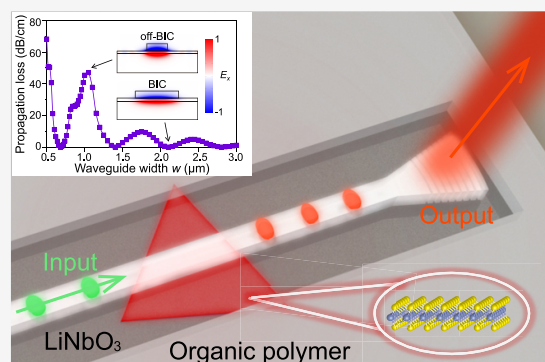
Read Online

| ACCESS | 📊 Metrics & More | 📄 Article Recommendations | 🔷 Supporting Information |

ABSTRACT: On-chip light sources are an essential component of scalable photonic integrated circuits (PICs), and coupling between light sources and waveguides has attracted a great deal of attention. Photonic waveguides based on bound states in the continuum (BICs) allow optical confinement in a low-refractive-index waveguide on a high-refractive-index substrate and thus can be employed for constructing PICs. In this work, we experimentally demonstrated that the photoluminescence (PL) from a monolayer of tungsten sulfide (WS$_2$) could be coupled into a BIC waveguide on a lithium-niobate-on-insulator (LNOI) substrate. Using finite-difference time-domain simulations, we numerically obtained a coupling efficiency of ∼2.3% for an in-plane-oriented dipole and a near-zero loss at a wavelength of 620 nm. By breaking through the limits of 2D-material integration with conventional photonic architectures, our work offers a new perspective for light−matter coupling in monolithic PICs.

KEYWORDS: bound states in the continuum, tungsten sulfide, photon emitters, lithium niobate on insulator

The term "bound states in the continuum (BICs)" refers to a type of perfectly confined waves that exist in a continuous spectrum of radiation, which was first introduced at the beginning of the 20th century by von Neumann and Wigner.[1] By introducing destructive interference between different dissipation mechanisms, the bound modes can be well confined in the continuum without leakage.[2] The concept of BICs has been confirmed in acoustics,[3,4] mechanics,[5,6] electronics,[7,8] and photonics.[9,10] On-chip photonic nanostructures have become a particularly appealing platform for research on BICs, especially as a result of the development of nanofabrication technology and integrated photonics. Photonic BICs have been found in a variety of optical structures, including waveguide arrays,[11] photonic crystals,[12] metasurfaces,[13] etc. The BIC-based photonic integrated circuits (PICs) on an etchless lithium niobate platform[14−16] have overcome a key challenge in traditional integrated photonics encountered during patterning single-crystal substrates. They have enabled many functional photonic devices, such as thermo-optical switches and filters, ultrafast photodetectors, and ultrafast electro-optic modulators.[17] The BIC-based etchless platform allows low-loss guiding of light and shows good fabrication tolerance for strong light−matter coupling,[18] which paves the way for scalable quantum photonic circuits.[2,19]
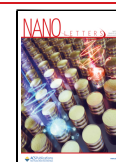
Single-photon emitters (SPEs) are the central building blocks for quantum PICs. SPEs have been investigated in various material systems, including quantum dots,[20−22] carbon nanotubes,[23,24] crystal color centers,[25,26] two-dimensional (2D) materials.[21,27] Among them, 2D materials are particularly appealing for large-scale integration and applications because they can be easily transferred and placed.[28−32] They have mechanical flexibility and are atomically thin compared with other systems,[27,33] allowing emitters to achieve a high extraction efficiency without total internal reflection.[34−36] However, to meet the demand for high refractive index contrast in optical waveguides, high-quality fabrication processes are required to pattern PICs on high-refractive-index substrates, which are usually very costly. For example, PICs based on silicon nitride require a well-controlled etch depth and smooth sidewall to achieve a minimum transmission loss of 1−2 dB/cm.[37] In addition, the pre/postfabricated PICs may introduce possible strain and distortion to the 2D materials.[38−40] Fortunately, BIC-based PICs provide an attractive route for integrating 2D materials with micro/nanostructures without the aforementioned challenges.[17] Therefore, integrating 2D materials on the etchless platform
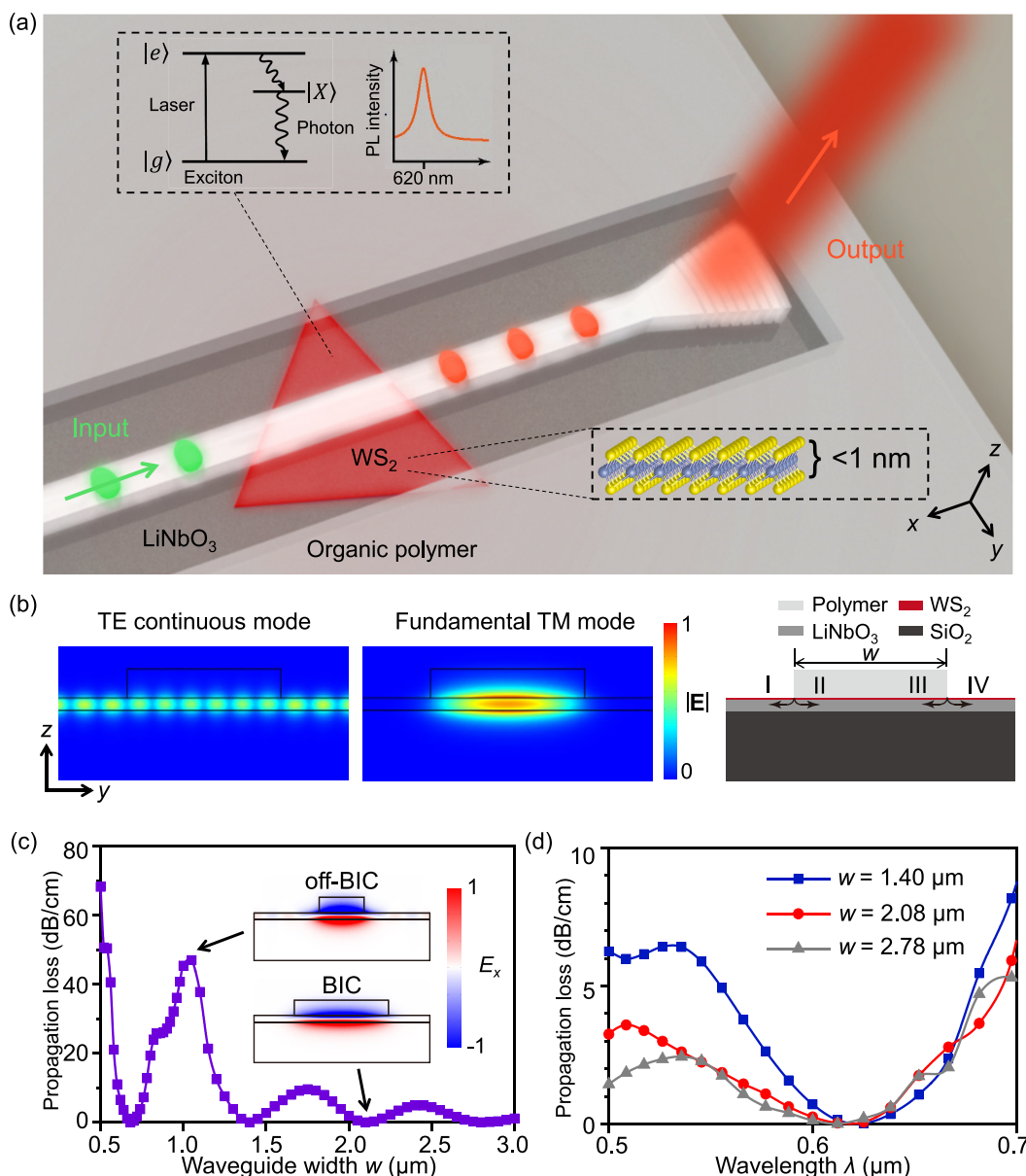
Figure 1. (a) Schematic of integrating monolayer WS_2 with a BIC photonic waveguide. The lower right inset shows the atomic structure of monolayer WS_2. The upper left inset shows the energy-level diagram and fluorescence spectrum of monolayer WS_2. (b) Left: cross-sectional electric field distributions of the TE continuous mode and the TM_0 bound mode (BIC mode) in the integrated waveguide. Right: cross-sectional structure of the waveguide. (c) Propagation loss of the TM_0 bound mode as a function of the waveguide width w at the wavelength $\lambda = 620$ nm. The insets show the electric field profiles for two typical waveguide widths. (d) Propagation loss spectra for three different waveguide widths satisfying the BIC condition, which correspond to the first three lowest points in c.

holds great promise in investigating photoluminescence and even on-chip single-photon emitters (SPEs).

Here, we demonstrated coupling between photon emitters in monolayer tungsten sulfide (WS_2) and a low-loss BIC mode on an etchless integrated platform. The monolayer WS_2 was wet transferred to the lithium niobate substrate before patterning the low-refractive-index waveguides. By tailoring the waveguide width, minimal propagation loss was achieved at the BIC point, and a maximal photoluminescence (PL) intensity of $\sim 3.7 \times 10^5$ counts/s was obtained in the experimental measurement. We further investigated the coupling efficiency between the BIC waveguide and the emitter in the visible band with finite-difference time-domain (FDTD) simulations and numerically obtained a coupling

efficiency of $\sim 2.3\%$ for an in-plane orientated dipole. The simulation results show that our device not only supports a wide wavelength range (several tens of nanometers) of low-loss light transmission but also allows robust coupling with the light source. More importantly, the demonstrated structure can be applied to various kinds of 2D materials due to the generic mechanism of BICs. Our work shows great promise for building on-chip single-photon emitters with large-scale BIC-based PICs without fabrication challenges and offers new insight into on-chip integrated quantum light sources.

Figure 1a displays a schematic illustration of integrating monolayer WS_2 with a polymer waveguide supporting BIC modes on a lithium niobate substrate. A continuous-wave (CW) laser beam was coupled into the waveguide through a
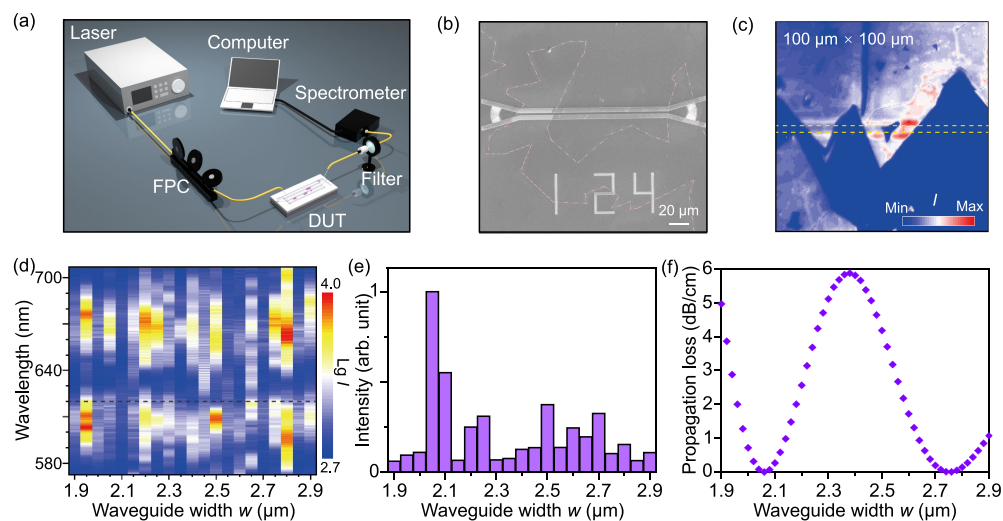
Figure 2. Demonstration of a BIC waveguide integrated with monolayer WS$_2$. (a) Experimental setup for measuring the WS$_2$-integrated BIC waveguide. FPC, fiber polarization controller; DUT, device under test. (b) Scanning electron microscope image of a WS$_2$-integrated BIC waveguide with two grating couplers. (c) Fluorescence intensity map measured with a confocal scanning microscope (excited with a 532 nm CW laser). The dashed lines indicate the position of the waveguide. (d) Normalized transmission intensity I as a function of the waveguide width w and laser wavelength λ. (e) Normalized PL intensity of collection as a function of the waveguide width w under the excitation of a 404 nm CW pump laser. (f) Simulated propagation loss at the wavelength of 620 nm as a function of the waveguide width w.

grating coupler (not shown) to excite the WS$_2$. The top left inset shows the PL process in our device under the excitation of a CW laser. The resulting PL was coupled into a BIC mode and then was stably transmitted through the waveguide and coupled to free space by another grating coupler. Specifically, the waveguide was constructed by patterning a fabrication-friendly optically transparent polymer (ZEP520A) on a z-cut LNOI substrate as shown in Figure 1b. Compared with other materials for integrated photonics, lithium niobate (LiNbO$_3$) has a wide transparency window from the visible to the infrared range (0.35 to 5 μm) and excellent linear/nonlinear optical properties.[41,42] The thicknesses of the lithium niobate layer, the polymer atop, and the silicon oxide underneath are 150 nm, 350 nm, and 2 μm, respectively. The monolayer WS$_2$ is atomically thin, and its interaction with the waveguide has little effect on the original BIC mode. Meanwhile, lithographic patterning of the polymer yields a negligible effect on the 2D material.[17] The proposed structure supports the transverse-magnetic (TM) bound modes, which are located in the transverse-electrical (TE) continuum. Usually, the fundamental TM (TM$_0$) mode is coupled to the TE continuum in the form of energy dissipation at the two edges of the waveguide through left-going (I, III) and right-going (II, IV) channels. By tailoring the waveguide width, one can obtain a BIC mode with zero propagation loss through introducing destructive interference between the energy dissipation channels.[15,18]

Since monolayer WS$_2$ has a peak PL intensity at 620 nm, the optical waveguide was designed to have minimal propagation loss at 620 nm. Figure 1c plots the simulated propagation loss of the TM$_0$ mode in a straight waveguide as a function of the waveguide width w at the wavelength of 620 nm (see details in the Supporting Information), which shows that the propagation loss approaches zero at specific widths (w = 0.68, 1.40, 2.08, and 2.78 μm). Furthermore, increase in w results in oscillating propagation loss with a decreased envelope, which is consistent with the theoretical analysis.[18] Figure 1d plots the propagation loss as a function of wavelength for w = 1.40, 2.08, and 2.78 μm, indicating a low-loss (<1 dB/cm) wavelength

range of >60 nm. This is attributed to the small structural dispersion, where photons are confined mainly in the LiNbO$_3$ thin film when propagating along the waveguide.

We fabricated straight waveguides with w ranging from 1.9 to 2.9 μm on a polymer/WS$_2$/LNOI hybrid platform . The monolayer WS$_2$ was wet-transferred onto a z-cut LNOI substrate after wafer cleaning with acetone and 2-propanol (see details in the Supporting Information). The polymer ZEP520A was spin-coated on the wafer at 4000 rpm for 1 min, and then prebaked on a hot plate at 180 °C for 3 min, resulting in a film thickness of 350 nm. The waveguide and grating couplers were defined in the polymer thin film by using a high-resolution electron-beam lithography system (Elionix ELS7800) with a dose of 180−220 μC/cm^2. After electron-beam exposure, the wafer was developed in ZED-N50 at 0 °C for 1 min, rinsed in a mixture of methyl isobutyl ketone and isopropyl alcohol (9:1) at room temperature for 30 s, and blow-dried.

Figure 2a shows our experimental setup for measuring the output PL spectra. Light from a 404 nm CW laser was sent through a fiber polarization controller (FPC) before being coupled into the device under test (DUT). The FPC was used for optimizing the coupling between the pump laser and the on-chip waveguide. Two fibers were mounted on the Thorlabs NanoMax six-axis flexure stage (MAX602D/M) with a 21° tilt angle to input the pump laser and collect the output PL via an input and output grating coupler, respectively. The TM-polarized light coupled from the laser into the waveguide excited the monolayer WS$_2$ and induced PL photons. (It should be noted here that the parameters of the waveguide and grating are optimized for λ = 620 nm, and the laser noise at the collection port is reduced.) Then, the PL was coupled into the TM$_0$ waveguide mode and further coupled into a single-mode fiber. To analyze the signal, we used a SP2500 spectrometer from Teledyne Princeton Instruments.

Figure 2b shows a scanning electron microscope (SEM) image of a typical WS$_2$-integrated BIC waveguide with a width of 2.75 μm and a length of 150 μm, where the pink dashed line
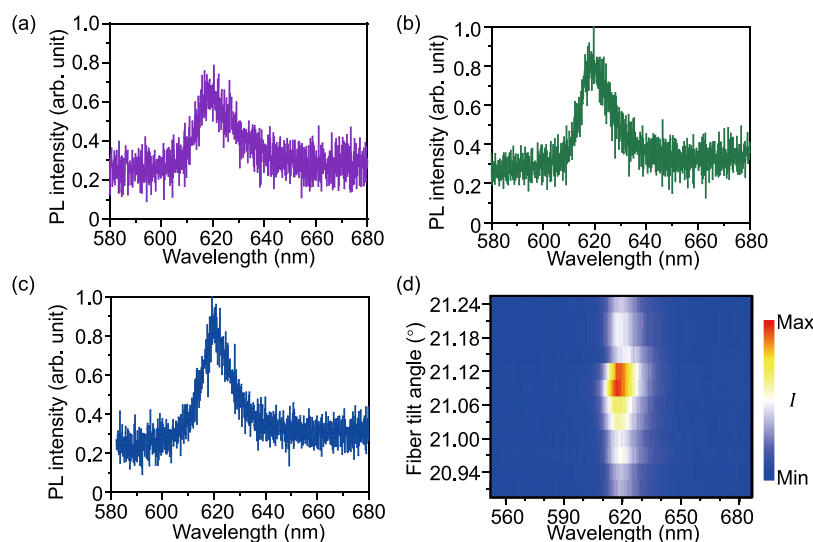
Figure 3. (a, b) PL spectra collected from monolayer WS$_2$ integrated with a BIC waveguide under the excitation of a (a) 404 nm and (b) 532 nm laser. (c) PL spectrum collected from bare WS$_2$ on a smooth substrate under the excitation of a 532 nm laser. (d) PL spectra collected from the integrated waveguide as a function of the fiber tilt angle.
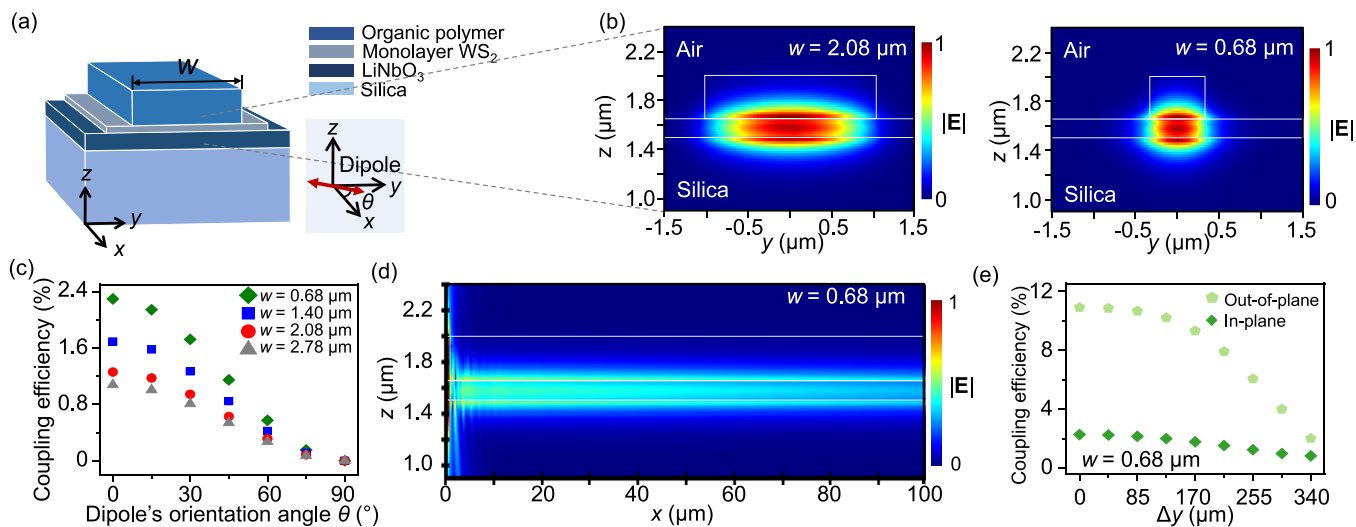

Figure 4. Three-dimensional FDTD simulation results of the coupling efficiency between the photon emitter and BIC waveguide. (a) Simulation model for the monolayer-WS$_2$-integrated BIC waveguide, where an in-plane dipole ($\lambda = 620$ nm) is placed inside the monolayer WS$_2$. The inset shows the defined orientation angle of the dipole. (b) Electric field distributions of the BIC mode coupled with a dipole source for structures with w = 2.08 μm (left) and w = 0.68 μm (right). (c) Coupling efficiency of an in-plane oriented dipole with a BIC waveguide as a function of the dipole's orientation angle θ, with the waveguide width w = 0.68, 1.40, 2.08, 2.78 μm. (d) Electric field distribution along a BIC waveguide (w = 0.68 μm) coupled with a dipole. The dipole is placed at (x, y, z) = (0.5 μm, 0, 1.65 μm). (e) Coupling efficiencies of an in-plane and out-of-plane oriented dipole with a BIC waveguide (w = 0.68 μm) as a function of misalignment Δy between the dipole and the y-center of the waveguide.

indicates the boundary of monolayer WS$_2$ for viewing convenience. It should be noted that the locations of the monolayer WS$_2$ under the waveguides are random for different samples. We also obtained the PL map of a WS$_2$-integrated BIC waveguide with a confocal scanning microscope, as shown in Figure 2c. The position of the polymer waveguide is indicated with yellow dashed lines (details in the Supporting Information).

We first characterized the propagation loss of the WS$_2$-integrated waveguides, with the waveguide width w varying from 1.9 to 2.9 μm. Figure 2d shows the measured optical transmission spectra for different waveguide widths, where maximal transmission (corresponding to minimal propagation loss) is achieved at certain waveguide widths. The high

transmission can maintain in a wavelength range spanning >30 nm, which is consistent with the simulated results in Figure 1d. Next, we measured the PL coupling phenomena in the WS$_2$-integrated waveguides with different waveguide widths (w) by using a 404 nm CW laser, with the results shown in Figure 2e. We observed the maximal PL intensity at w = 2.05 μm, which is attributed to the fact that the TM bound mode can be decoupled completely from the continuum modes at this width. Relatively high PL intensity was also obtained at a waveguide width near 2.70 μm, which is another BIC point. For comparison, Figure 2f shows the propagation loss of the waveguide as a function of the waveguide width w. The trend of PL transmission with the waveguide width is consistent in both experiment and simulation, which proves that the

photons emitted from monolayer WS_2 can be coupled into a BIC mode. The slight deviation in the experiment is attributed mainly to the uncontrollable position and size of the monolayer WS_2 integrated with the waveguide in each device. The dipole's position (especially along the y direction) affects the coupling efficiency between the dipole and the guided TM mode, and a maximal coupling efficiency can be obtained when the misalignment Δy is within ± 100 nm (details in Figure 4). Since the WS_2's size determines the total number of dipoles, by choosing larger waveguide width, one can have more dipoles coupled with the guided TM mode, which leads to a stronger PL signal. In addition, the fabrication deviation in the device's geometry, the misalignment between the grating couplers and fibers, and the vibration of the measurement platform also cause performance deterioration.

To further confirm that the collected signal is emitted from monolayer WS_2, we compared the measurement results from the integrated waveguide with those from the bare monolayer WS_2. Figure 3a-c shows the measured PL spectra from a bare WS_2 thin film under the excitation of a 532 nm laser (blue line) and from a WS_2-integrated BIC waveguide ($w = 2.05$ μm) under the excitation of a 532 nm laser (green line) and a 404 nm laser (purple line). The measured central wavelengths and full widths at half-maximum of the peaks in the PL spectra are consistent, indicating that the photons collected from the integrated waveguide are from the fluorescence of WS_2. The PL intensity collected from a WS_2-integrated BIC waveguide via a grating coupler is on the same order of magnitude as that collected from bare WS_2 via an objective lens (100×, NA = 0.9). However, a direct comparison of the PL efficiencies is not recommended due to several factors, e.g., the uncontrollable position and size of the WS_2 monolayer, the coupling efficiency between the dipole and the guided mode, etc. Figure 3d shows the PL spectra measured from the same WS_2-integrated BIC waveguide as a function of the fiber tilt angle. The collected PL intensities are the highest at fiber tilt angles between 21.09° and 21.12°. The PL collection efficiency has a strong dependence on the fiber tilt angle because the intensity drops to 65% (45%) of the original as the angle moves only 0.03° away to the positive (negative) side. The results also indicate that the grating coupler may affect the collected PL center wavelength by 2−3 nm due to the wavelength-dependent coupling efficiency.

We also estimated the coupling efficiency between the BIC waveguide and monolayer WS_2 with FDTD simulations, as shown in Figure 4. Note that, we could not adopt a macroscopic model for the monolayer 2D material in FDTD simulations due to the mesh division constraint (20 nm), which is much larger than the monolayer thickness (<1 nm). Instead, we treated the photons emitted from the monolayer as electric dipoles with in-plane orientation. We placed a dipole source at the intersection of the polymer waveguide and the $LiNbO_3$ thin film. The dipole source orientation was restricted in the x-y plane, where the angle between the orientation and the x-axis (along the waveguide direction) is defined as θ, as shown in the inset of Figure 4a. The dipole wavelength (620 nm) was set to be consistent with that of the monolayer WS_2. To be consistent with our experiments, we considered the coupling efficiency only at one end of the waveguide, while the other end is used for excitation. Figure 4b shows the electric field distributions of the TM_0 mode at $w = 2.08$ μm (left) and $w = 0.68$ μm (right), both of which satisfy the BIC condition. For comparison, we calculated the coupling efficiencies

between the dipole source and the TM_0 mode at $w = 0.68$, 1.40, 2.08, and 2.78 μm, all satisfying the BIC condition. The coupling efficiency is 2.3% at $w = 0.68$ μm (after propagating along the waveguide for 4 μm) and decreases as the waveguide width w increases. Since a waveguide with a larger waveguide width can support more high-order TM modes, we also investigated the coupling efficiency for TM modes of different orders (see the Supporting Information). We also numerically simulated the TM_0 coupling efficiency as a function of the electric dipole orientation θ at different waveguide widths satisfying the BIC condition with the results shown in Figure 4c. The coupling efficiency increases as θ decreases and reaches a maximum at $\theta = 0°$ (along the x axis), which is different from the case for the coupling between the TE mode and the 2D materials.[31]

Based on FDTD simulation, the BIC mode for $w = 0.68$ μm has superior modal matching with the dipole compared to the BIC mode with $w = 2.08$ μm due to the small dipole mode ($\lambda = 620$ nm), and its coupling efficiency is 2.11 times that for $w = 2.08$ μm. Thus, we then focused on the structure with a waveguide width of $w = 0.68$ μm to seek further improvement in the coupling efficiency. Figure 4d depicts the cross-sectional (x-z plane) electric field distribution of the BIC waveguide coupled with a dipole, where the dipole is placed near the waveguide end ($x = 0$) and at the waveguide's y-center with the coordinates $(x, y, z) = (0.5$ μm, 0, 1.65 μm) and orientation angle $\theta = 0°$. It is clear that the light emitted by the dipole can be coupled to the waveguide for a 100 μm propagation length. The leakage along the z direction is attributed mainly to a poor match between the radiation mode of the in-plane dipole and the TM-polarized BIC mode of the waveguide. In this connection, we also simulated the coupling efficiency of the out-of-plane dipole with the BIC waveguide, which as shown in Figure 4e can reach 10.9%, approximately five times that of an in-plane dipole. Therefore, the BIC waveguide shows great promise for integration with thin layered materials with an out-of-plane dipole orientation. In addition, Figure 4e shows that the coupling efficiency is almost unaffected by a < 100 nm displacement of the dipole in the y direction, which indicates a good fabrication tolerance of this integration scheme. Therefore, our structure can achieve a high coupling efficiency with the WS_2 PL that is insensitive to the photon emitter's position. It is expected that more complicated nanostructures such as a high-quality cavity based on a hybrid-integrated BIC waveguide will enhance the coupling efficiency further.

In conclusion, we experimentally realized on-chip photon emitters by integrating monolayer WS_2 with a BIC waveguide. Specifically, the structure consists of a monolayer WS_2 sandwiched between a polymer waveguide (with a low refractive index) and a $LiNbO_3$ thin film (with a high refractive index). This structure allows the PL of monolayer WS_2 to be coupled to the to be coupled to the film an and transmitted along the waveguide. The device fabrication does not include the etching of $LiNbO_3$, which minimizes the possibility of damaging the monolayer WS_2 and considerably reduces the fabrication cost and difficulty. In addition, our structure shows a low-loss (<1 dB/cm) wavelength range of >60 nm and insensitivity to the position of the photon emitters. Although the coupling with the TM-polarized BIC is limited because of the orientation of the photon emitters in WS_2, FDTD simulation results show that the coupling efficiency of the fluorescence with the BIC mode can be further improved by choosing a narrower waveguide width. A

coupling efficiency as high as 10.9% can be achieved from an out-of-plane-oriented dipole, which is promising for potential applications using emitters with an out-of-plane polarization in a thin layered material. In addition, special nanostructures such as nanocavities, metasurfaces, Bragg gratings, etc., can further enhance the emission intensity and coupling efficiency.[43−45] Due to the generic mechanism of BICs and wide transparency band of LiNbO$_3$, our structure can be extended directly to all monolayer 2D materials, thus enabling a wide range of applications. Our work provides a new insight for 2D-material-integrated photonics on an LNOI platform and enables integration of deterministic single-photon emitters on integrated photonic platforms without fabrication challenges, which will promote the development of on-chip quantum information processing and quantum networks.

■ ASSOCIATED CONTENT

Ⓢ🅸 Supporting Information

The Supporting Information is available free of charge at https://pubs.acs.org/doi/10.1021/acs.nanolett.2c05034.

> Additional experimental details: calculation of the propagation loss in a straight waveguide, growth of monolayer WS$_2$, wet transfer process, precharacterized PL map of the waveguide, transmittance measurement of the grating coupler, setup for characterizing the WS$_2$-integrated BIC waveguide, and simulation results of the coupling efficiency (PDF)

■ AUTHOR INFORMATION

Corresponding Authors

Xi-Feng Ren − *CAS Key Laboratory of Quantum Information, University of Science and Technology of China, Hefei 230026, China; CAS Center for Excellence in Quantum Information and Quantum Physics, University of Science and Technology of China, Hefei 230026, China; Hefei National Laboratory, University of Science and Technology of China, Hefei 230088, China;* ⓞ orcid.org/0000-0001-6559-8101; Email: renxf@ustc.edu.cn

Xiankai Sun − *Department of Electronic Engineering, The Chinese University of Hong Kong, Shatin, Hong Kong SAR, China;* ⓞ orcid.org/0000-0002-9137-0298; Email: xksun@cuhk.edu.hk

Authors

Xiao-Jing Liu − *CAS Key Laboratory of Quantum Information, University of Science and Technology of China, Hefei 230026, China; CAS Center for Excellence in Quantum Information and Quantum Physics, University of Science and Technology of China, Hefei 230026, China; Hefei National Laboratory, University of Science and Technology of China, Hefei 230088, China*

Yue Yu − *Department of Electronic Engineering, The Chinese University of Hong Kong, Shatin, Hong Kong SAR, China*

Di Liu − *CAS Key Laboratory of Quantum Information, University of Science and Technology of China, Hefei 230026, China; CAS Center for Excellence in Quantum Information and Quantum Physics, University of Science and Technology of China, Hefei 230026, China; Hefei National Laboratory, University of Science and Technology of China, Hefei 230088, China*

Qi-Long Cui − *National Synchrotron Radiation Laboratory, CAS Center for Excellence in Nanoscience, University of Science and Technology of China, Hefei, Anhui 230029, China*

Xiaozhuo Qi − *School of Physical Science and Technology, Tiangong University, Tianjin 300387, China*

Yang Chen − *CAS Key Laboratory of Quantum Information, University of Science and Technology of China, Hefei 230026, China; CAS Center for Excellence in Quantum Information and Quantum Physics, University of Science and Technology of China, Hefei 230026, China; Hefei National Laboratory, University of Science and Technology of China, Hefei 230088, China*

Guangyuan Qu − *School of Physical Sciences, University of Science and Technology of China, Hefei, Anhui 230026, China*

Li Song − *National Synchrotron Radiation Laboratory, CAS Center for Excellence in Nanoscience, University of Science and Technology of China, Hefei, Anhui 230029, China;* ⓞ orcid.org/0000-0003-0585-8519

Guo-Ping Guo − *CAS Key Laboratory of Quantum Information, University of Science and Technology of China, Hefei 230026, China; CAS Center for Excellence in Quantum Information and Quantum Physics, University of Science and Technology of China, Hefei 230026, China; Hefei National Laboratory, University of Science and Technology of China, Hefei 230088, China;* ⓞ orcid.org/0000-0002-2179-9507

Guang-Can Guo − *CAS Key Laboratory of Quantum Information, University of Science and Technology of China, Hefei 230026, China; CAS Center for Excellence in Quantum Information and Quantum Physics, University of Science and Technology of China, Hefei 230026, China; Hefei National Laboratory, University of Science and Technology of China, Hefei 230088, China*

Complete contact information is available at:
https://pubs.acs.org/10.1021/acs.nanolett.2c05034

Author Contributions

△X.-J.L. and Y.Y. contributed equally to this work

Notes

The authors declare no competing financial interest.

■ ACKNOWLEDGMENTS

■ REFERENCES

(1) Von Neumann, J.; Wigner, E. On some peculiar discrete eigenvalues. *Phys. Z.* **1929**, *30*, 465−467.

(2) Hsu, C. W.; Zhen, B.; Stone, A. D.; Joannopoulos, J. D.; Soljačić, M. Bound states in the continuum. *Nat. Rev. Mater.* **2016**, *1*, 16048.

(3) Linton, C. M.; McIver, P. Embedded trapped modes in water waves and acoustics. *Wave Motion* **2007**, *45*, 16−29.

(4) Lyapina, A. A.; Maksimov, D. N.; Pilipchuk, A. S.; Sadreev, A. F. Bound states in the continuum in open acoustic resonators. *J. Fluid Mech.* **2015**, *780*, 370−387.

(5) Tong, H.; Liu, S.; Zhao, M.; Fang, K. Observation of phonon trapping in the continuum with topological charges. *Nat. Commun.* **2020**, *11*, 5216.

(6) Yu, Y.; Xi, X.; Sun, X. Observation of mechanical bound states in the continuum in an optomechanical microresonator. *Light Sci. Appl.* **2022**, *11*, 328.

(7) Capasso, F.; Sirtori, C.; Faist, J.; Sivco, D. L.; Chu, S. N. G.; Cho, A. Y. Observation of an electronic bound state above a potential well. *Nature* **1992**, *358*, 565−567.

(8) Gong, W.; Han, Y.; Wei, G. Antiresonance and bound states in the continuum in electron transport through parallel-coupled quantum-dot structures. *Phys.: Condens. Matter* **2009**, *21*, 175801.

(9) Marinica, D. C.; Borisov, A. G.; Shabanov, S. V. Bound states in the continuum in photonics. *Phys. Rev. Lett.* **2008**, *100*, 183902.

(10) Gomis-Bresco, J.; Artigas, D.; Torner, L. Anisotropy-induced photonic bound states in the continuum. *Nat. Photonics* **2017**, *11*, 232−236.

(11) Plotnik, Y.; Peleg, O.; Dreisow, F.; Heinrich, M.; Nolte, S.; Szameit, A.; Segev, M. Experimental observation of optical bound states in the continuum. *Phys. Rev. Lett.* **2011**, *107*, 183901.

(12) Gansch, R.; Kalchmair, S.; Genevet, P.; Zederbauer, T.; Detz, H.; Andrews, A. M.; Schrenk, W.; Capasso, F.; Loncar, M.; Strasser, G. Measurement of bound states in the continuum by a detector embedded in a photonic crystal. *Light Sci. Appl.* **2016**, *5*, e16147.

(13) Liang, Y.; Koshelev, K.; Zhang, F.; Lin, H.; Lin, S.; Wu, J.; Jia, B.; Kivshar, Y. Bound states in the continuum in anisotropic plasmonic metasurfaces. *Nano Lett.* **2020**, *20*, 6351−6356.

(14) Yu, Z.; Xi, X.; Ma, J.; Tsang, H. K.; Zou, C. L.; Sun, X. Photonic integrated circuits with bound states in the continuum. *Optica* **2019**, *6*, 1342−1348.

(15) Yu, Z.; Sun, X. Acousto-optic modulation of photonic bound state in the continuum. *Light Sci. Appl.* **2020**, *9*, 1.

(16) Yu, Y.; Yu, Z.; Wang, L.; Sun, X. Ultralow-Loss Etchless Lithium Niobate Integrated Photonics at Near-Visible Wavelengths. *Adv. Opt. Mater.* **2021**, *9*, 2100060.

(17) Yu, Z.; Wang, Y.; Sun, B.; Tong, Y.; Xu, J. B.; Tsang, H. K.; Sun, X. Hybrid 2D-Material Photonics with Bound States in the Continuum. *Adv. Opt. Mater.* **2019**, *7*, 1901306.

(18) Zou, C. L.; Cui, J. M.; Sun, F. W.; Xiong, X.; Zou, X. B.; Han, Z. F.; Guo, G. C. Guiding light through optical bound states in the continuum for ultrahigh-Q microresonators. *Laser Photon. Rev.* **2015**, *9*, 114−119.

(19) Azzam, S. I.; Shalaev, V. M.; Boltasseva, A.; Kildishev, A. V. Formation of bound states in the continuum in hybrid plasmonic-photonic systems. *Phys. Rev. Lett.* **2018**, *121*, 253901.

(20) Wu, Y. K.; Liu, X. J.; Qi, X. Z.; Lu, L.; Guo, G. P.; Guo, G. C.; Ren, X. F. Near-field modulation of single photon emitter with a plasmonic probe. *Appl. Phys. Lett.* **2021**, *118*, 104002.

(21) Liu, X.; Wu, Y.; Qi, X.; Lu, L.; Li, M.; Zou, C.; Ren, S.; Guo, G.; Guo, G.; Zhu, W.; Ren, X. Near-Field Modulation of Differently Oriented Single Photon Emitters with A Plasmonic Probe. *Nano Lett.* **2022**, *22*, 2244−2250.

(22) Kim, J. H.; Aghaeimeibodi, S.; Richardson, C. J. K.; Leavitt, R. P.; Englund, D.; Waks, E. Hybrid integration of solid-state quantum emitters on a silicon photonic chip. Nano letters. *Nano Lett.* **2017**, *17*, 7394−7400.

(23) Khasminskaya, S.; Pyatkov, F.; Słowik, K.; Ferrari, S.; Kahl, O.; Kovalyuk, V.; Rath, P.; Vetter, A.; Hennrich, F.; Kappes, M. M.; Gol'tsman, G.; Korneev, A.; Rockstuhl, C.; Krupke, R.; Pernice, W. H. P. Fully integrated quantum photonic circuit with an electrically driven light source. *Nat. Photonics* **2016**, *10*, 727−732.

(24) He, X.; Htoon, H.; Doorn, S. K.; Pernice, W. H. P.; Pyatkov, F.; Krupke, R.; Jeantet, A.; Chassagneux, Y.; Voisin, C. Carbon nanotubes as emerging quantum-light sources. *Nat. Mater.* **2018**, *17*, 663−670.

(25) Doherty, M. W.; Manson, N. B.; Delaney, P.; Jelezko, F.; Wrachtrup, J.; Hollenberg, L. C. L. The nitrogen-vacancy colour centre in diamond. *Phys. Rep.* **2013**, *528*, 1−45.

(26) Hollenbach, M.; Berencen, Y.; Kentsch, U.; Helm, M.; Astakhov, G. V. Engineering telecom single-photon emitters in silicon for scalable quantum photonics. *Opt. Express* **2020**, *28*, 26111−26121.

(27) Palacios-Berraquero, C.; Kara, D. M.; Montblanch, A. R. P.; Barbone, M.; Latawiec, P.; Yoon, D.; Ott, A. K.; Loncar, M.; Ferrari, A. C.; Atatüre, M. Large-scale quantum-emitter arrays in atomically thin semiconductors. *Nat. Commun.* **2017**, *8*, 15093.

(28) Chakraborty, C.; Vamivakas, N.; Englund, D. Advances in quantum light emission from 2D materials. *Nanophotonics* **2019**, *8*, 2017−2032.

(29) Elshaari, A. W.; Skalli, A.; Gyger, S.; Nurizzo, M.; Schweickert, L.; Zadeh, I. E.; Svedendahl, M.; Steinhauer, S.; Zwiller, V. Deterministic integration of hBN emitter in silicon nitride photonic waveguide. *Adv. Quantum Technol.* **2021**, *4*, 2100032.

(30) Peyskens, F.; Chakraborty, C.; Muneeb, M.; Van Thourhout, D.; Englund, D. Integration of single photon emitters in 2D layered materials with a silicon nitride photonic chip. *Nat. Commun.* **2019**, *10*, 4435.

(31) Kim, S.; Duong, N. M. H.; Nguyen, M.; Lu, T. J.; Kianinia, M.; Mendelson, N.; Solntsev, A.; Bradac, C.; Englund, D. R.; Aharonovich, I. Integrated on chip platform with quantum emitters in layered materials. *Adv. Opt. Mater.* **2019**, *7*, 1901132.

(32) Zhang, Q.; Hu, G.; Ma, W.; Li, P.; Krasnok, A.; Hillenbrand, R.; Alù, A.; Qiu, C. W. Interface nano-optics with van der Waals polaritons. *Nature* **2021**, *597*, 187−195.

(33) Cai, T.; Dutta, S.; Aghaeimeibodi, S.; Yang, Z.; Nah, S.; Fourkas, J. T.; Waks, E. Coupling emission from single localized defects in two-dimensional semiconductor to surface plasmon polaritons. *Nano Lett.* **2017**, *17*, 6564−6568.

(34) Aharonovich, I.; Englund, D.; Toth, M. Solid-state single-photon emitters. *Nat. Photonics* **2016**, *10*, 631−641.

(35) Gould, M.; Schmidgall, E. R.; Dadgostar, S.; Hatami, F.; Fu, K. M. C. Efficient extraction of zero-phonon-line photons from single nitrogen-vacancy centers in an integrated gap-on-diamond platform. *Phys. Rev. Appl.* **2016**, *6*, 011001.

(36) Vogl, T.; Campbell, G.; Buchler, B. C.; Lu, Y.; Lam, P. K. Fabrication and deterministic transfer of high-quality quantum emitters in hexagonal boron nitride. *ACS Photon.* **2018**, *5*, 2305−2312.

(37) Ren, S.; Yan, W.; Feng, L.; Chen, Y.; Wu, Y.; Qi, X.; Liu, X.; Cheng, Y.; Xu, B.; Deng, L.; Guo, G.; Bi, L.; Ren, X. Single-Photon Nonreciprocity with an Integrated Magneto-Optical Isolator. *Laser Photonics Rev.* **2022**, *16*, 2100595.

(38) Katsumi, R.; Ota, Y.; Osada, A.; Tajiri, T.; Yamaguchi, T.; Kakuda, M.; Iwamoto, S.; Akiyama, H.; Arakawa, Y. In situ wavelength tuning of quantum-dot single-photon sources integrated on a CMOS-processed silicon waveguide. *Appl. Phys. Lett.* **2020**, *116*, 041103.

(39) Katsumi, R.; Ota, Y.; Kakuda, M.; Iwamoto, S.; Arakawa, Y. Transfer-printed single-photon sources coupled to wire waveguides. *Optica* **2018**, *5*, 691−694.

(40) Lin, H.; Song, Y.; Huang, Y.; Kita, D.; Deckoff-Jones, S.; Wang, K.; Li, L.; Li, J.; Zheng, H.; Luo, Z.; Wang, H.; Novak, S.; Yadav, A.; Huang, C. C.; Shiue, R. J.; Englund, D.; Gu, T.; Hewak, D.; Richardson, K.; Kong, J.; Hu, J. Chalcogenide glass-on-graphene photonics. *Nat. Photonics* **2017**, *11*, 798−805.

(41) Zhou, J.; Liang, Y.; Liu, Z.; Chu, W.; Zhang, H.; Yin, D.; Fang, Z.; Wu, R.; Zhang, J.; Chen, W.; Wang, Z.; Zhou, Y.; Wang, M.; Cheng, Y. On-Chip Integrated Waveguide Amplifiers on Erbium-Doped Thin-Film Lithium Niobate on Insulator. *Laser Photon. Rev.* **2021**, *15*, 2100030.

(42) Arizmendi, L. Photonic applications of lithium niobate crystals. *Phys. Stat. Sol.(A)* **2004**, *201*, 253−283.

(43) Xu, Y.; Wang, F.; Gao, Y.; Chen, W.; Chen, C.; Wang, X.; Yi, Y.; Sun, X.; Zhang, D. Efficient polymer waveguide grating coupler with directionality enhancement. *Opt. Commun.* **2020**, *463*, 125418.

(44) Zhang, W.; Yao, J. A fully reconfigurable waveguide Bragg grating for programmable photonic signal processing. *Nat. Commun.* **2018**, *9*, 1396.

(45) Shao, L.; Maity, S.; Zheng, L.; Wu, L.; Shams-Ansari, A.; Sohn, Y. I.; Puma, E.; Gadalla, M. N.; Zhang, M.; Wang, C.; Hu, E.; Lai, K.; Lončar, M. Phononic band structure engineering for high-Q gigahertz surface acoustic wave resonators on lithium niobate. *Phys. Rev. Appl.* **2019**, *12* (1), 014022.

📖 Recommended by ACS

Nanocavity-Integrated van der Waals Heterobilayers for Nano-excitonic Transistor

Yeonjeong Koo, Kyoung-Duck Park, *et al.*

MARCH 01, 2023
ACS NANO   READ 🔗

Exciton–Photon Interactions in Two-Dimensional Semiconductor Microcavities

Jingzhi Shang, Ting Yu, *et al.*

FEBRUARY 13, 2023
ACS PHOTONICS   READ 🔗

WSe$_2$ Light-Emitting Device Coupled to an h-BN Waveguide

Ronja Khelifa, Lukas Novotny, *et al.*

MARCH 23, 2023
ACS PHOTONICS   READ 🔗

WS$_2$–Flake-Sandwiched, Au-Nanodisk-Enabled High-Quality Fabry–Pérot Nanoresonators for Photoluminescence Modulation

He Huang, Jianfang Wang, *et al.*

AUGUST 29, 2022
ACS NANO   READ 🔗

Get More Suggestions >